Water Science & Technology

IWA PUBLISHING

Water Science & Technology Vol 88 No 8, 1944 doi: 10.2166/wst.2023.327

Effective removal of Cr(VI) in water by bulk-size polyaniline/polyvinyl alcohol/amyloid fibril composite beads

Jia Wen [a,b,c,*], Yuru Zhang[b,c] and Yinlin Du[b,c]

[a] Research Institute of Hunan University in Chongqing, Chongqing 401120, China
[b] College of Environmental Science and Engineering, Hunan University, Changsha 410082, China
[c] Key Laboratory of Environmental Biology and Pollution Control (Hunan University), Ministry of Education, Changsha 410082, China
*Corresponding author. E-mail: jwen@hnu.edu.cn

JW, 0000-0003-1970-5329

ABSTRACT

With the rapid expansion of industrial activities, chromium ions are discharged into the environment and cause water and soil pollution of various extents, which seriously endangers the natural ecological environment and human health. In this study, polyaniline/polyvinyl alcohol/amyloid fibril (PANI/PVA/AFL) composite gel beads (PPA) were prepared from polyaniline and amyloid fibrils with HCl as doping acid and PVA as a cross-linking agent. The results showed that PPA was an irregular composite bead with a diameter of 6 mm. The adsorption of Cr(VI) on the PPA gel beads followed the pseudo-second-order kinetics model, suggesting that chemical reactions were the controlling step in the Cr(VI) adsorption process. Though the Redlich–Peterson isotherm model had the best fit for the adsorption data, the isothermal adsorption process can be simplified using the Langmuir model. The maximum adsorption capacity for Cr(VI) in water was 51.5 mg g^{-1}, comparable to or even higher than some PANI-based nanomaterials. Thermodynamic parameters showed that the adsorption process was a spontaneous, endothermic, and entropy-increasing process. Microscopic analysis revealed that the capture of Cr(VI) on PPA was mainly governed by electrostatic attraction, reduction, and complexation reactions. PPA can be used as a kind of effective remediation agent to remove Cr(VI) in water.

Key words: adsorption, amyloid fibril, chromium, polyaniline, redox reaction

HIGHLIGHTS

- PPA gel beads with bulk sizes were synthesized to remediate Cr(VI) in water.
- Adsorption kinetics, isotherms, and thermodynamics of Cr on the PPA gel beads were studied.
- PPA showed a high adsorption capacity (51.5 mg g^{-1}) for Cr(VI).
- Cr(VI) was almost completely reduced to Cr(III) on the PPA beads.
- Electrostatic attraction, reduction, and complexation occurred for the Cr(VI) removal.

1. INTRODUCTION

As an important industrial metal element, chromium (Cr) is widely used in electroplating, metallurgy, leather tanning, and other industries (Gao & Xia 2011). Due to the rapid expansion of these industrial activities, Cr ions are also discharged into the environment in large quantities along with industrial wastewater, which has caused serious heavy metal pollution of water and soil and seriously harmed the natural ecological environment and human health (Peng *et al.* 2009; Kapoor *et al.* 2022). Chromium in a water environment mainly exists as trivalent chromium (Cr(III)) and hexavalent chromium (Cr(VI)). Cr(III) is the most stable oxidation state form of chromium in living organisms and the main form of chromium in living organisms. It is easy to form multi-tooth coordination compounds, but it is not easy to cross the cell membrane and has low reactivity. It is one of the essential trace elements in human and animal bodies. However, Cr(VI) easily crosses the cell membrane and reacts with nucleic acid and protein components, causing oxidative stress, DNA damage, cell apoptosis, or gene mutation in the cell, so it has carcinogenic and mutagenic effects (Wang *et al.* 2021). Therefore, a widely acknowledged way of reducing Cr(VI) toxicity is to convert its Cr(VI) forms to the less toxic Cr(III) forms and then make

them stabilized. In water treatment, using reductants such as ferrites (Wu *et al.* 2022), zero-valent iron (Quan *et al.* 2014; Zhang *et al.* 2018; Liu *et al.* 2022), sulfides (Wang *et al.* 2019, 2020), or other materials with reducing ability (Chrysochoou & Reeves 2017; Sangeetha *et al.* 2019; Farooqi *et al.* 2021; Dong *et al.* 2023) has been proved efficient in Cr detoxification.

In recent years, polyaniline (PANI) has been applied in conductive adhesives (Derakhshankhah *et al.* 2020), rechargeable batteries (Cui *et al.* 2020), sensors (Anantha-Iyengar *et al.* 2019), corrosion-resistant material (Perumal *et al.* 2020), and pollutant adsorbent (Mahanta *et al.* 2009; Wang *et al.* 2009; Guo *et al.* 2011) due to its good environmental stability, biocompatibility, and low production cost. Polyaniline molecules contain a large number of reducing amine (-NH -) and oxidizing imine (-N=) groups, which not only have an excellent complexing effect on heavy metal ions (Liu & Huang 2011; Peydayesh *et al.* 2019) but also react with some heavy metal ions with high oxidation potential (such as Cr) (Leung *et al.* 2013). Polyaniline can be divided into a reducing state, an oxidation state, and eigenstate according to the proportion of amine and imine groups. During the reaction with Cr(VI), the electron energy is transferred from the reduced state and the eigenstate to the oxidation state, thus promoting the reduction of Cr(VI) to Cr(III) (Li *et al.* 2020). Polyaniline has been widely used in the remediation of Cr pollution in water. Zhang *et al.* (2010) and Wang *et al.* (2014) studied the removal effect of polyaniline doped with sulfuric acid and hydrochloric acid on Cr(VI) in water. The maximum adsorption capacity of the two kinds of polyanilines for Cr(VI) was 95.79 and 182 mg g^{-1}, respectively. The redox potential (E_0) of Cr(VI) in the acidic condition is much higher than that in the alkaline condition, thus accelerating the redox reaction of Cr(VI) with the amine group (Ding *et al.* 2018). The acidic environment can also protonate the amine group on polyaniline and promote the electrostatic attraction between it and Cr(VI) (mainly $HCrO_4^-$). SO_4^{2-} or Cl^- on polyaniline will then undergo anion exchange with $HCrO_4^-$ to remove chromium from the solution (Zhang *et al.* 2018).

Most adsorbents used in water purification are nano-size materials that exhibit outstanding performance in metal removal. However, their small size also endows them inactivity owing to the nanomaterial's aggregation phenomenon in solution. Nanomaterials also suffer from the great impediment of separation and recycling. Thus, they need to be grafted onto some stable and larger-size material, such as biochar (Chen *et al.* 2021, 2022) and graphene oxide (Kong *et al.* 2019), to prevent losing efficiency and facilitate recycling. Similarly, polyaniline presents in a powder form of a nano- or micro-size structure. Loading polyaniline on stable and big-size supporters will conduce to their removal effect. Recently, the design of bulk-sized materials has caught much attention because they can fix the problems mentioned above with the merits of easy collection, non-aggregation, and non-secondary pollution. However, the major limitation of normal bulk-sized materials for Cr removal is their low adsorption capacities due to limited surface area and porosity. For example, the maximum adsorption capacity (Q_{max}) was reported in some studies using bulk-sized materials: 6.31 mg g^{-1} for surfactant-modified zeolites (0.12–0.18 mm) (Song *et al.* 2015), 3.40–28.88 mg g^{-1} for chitosan cross-linked silicon materials (0.075–0.25 mm) (Shi *et al.* 2017), 12.2 mg g^{-1} for PANI@PS gel beads of 0.4–0.6 mm (Ding *et al.* 2018), and 3.82 mg g^{-1} for IPS-AR gel beads of 5 mm (Lv *et al.* 2013). Therefore, it is necessary to design a bulk material with an adsorption capacity comparable to many existing nano- or micro-sized materials.

We noticed that β-lactoglobulin (β-LG) is the main protein in whey, a byproduct of the cheese industry, and is therefore cheap and readily available (Ramírez-Rodríguez *et al.* 2020). Protein amyloid fibrils (AFLs) can be obtained from β-LG by combining hydrolysis and aggregation of the original protein folding sequence at low pH and high temperature (Godiya *et al.* 2020). AFL has high fibrosis, strength, and thermochemical stability, and its surface is rich in natural amino acid groups, which have a strong affinity for Cr(VI) (Arputharaj *et al.* 2021). In addition, the aerogel derived from the AFL matrix has an abundant porous structure (porosity ~ 97%) (Peydayesh *et al.* 2020). AFL can be cross-linked with the amine group in PANI. Thus, AFL/PANI adsorbent can be prepared by a simple one-step chemical cross-linking method (Liu & Huang 2011). Studies have shown that the combination of AFL and polyvinyl alcohol (PVA) can not only overcome their respective shortcomings to form a regular shape of the material but also, through the physical and chemical double cross-linking, the composite can show better mechanical properties and chemical stability (Han *et al.* 2020). To our knowledge, there has been no study on establishing macroscopic bulk materials using the combination of PANI, PVA, and AFL. The mixture of AFL, PANI, and PVA to form solid bulk composite material is expected to greatly improve its structural stability and recovery value and synergistically improve the overall adsorption performance.

Therefore, the objectives of the study aimed to investigate: (a) the synthesis route of PANI, PVA, and AFL composite (hereafter named polyaniline/polyvinyl alcohol/amyloid fibril (PPA) composite beads); (b) the removal efficiency of PPA for Cr(VI) and Cr(VI) adsorption behaviors (kinetics, thermodynamics, and adsorption isotherms); and (c) examine the removal mechanisms associated with the adsorption process. The study will provide insight into using bulk materials for Cr remediation in the environment.

2. METHODS AND MATERIALS

2.1. Synthesis of polyaniline

Polyaniline was prepared with hydrochloric acid (HCl) as doping acid. The specific method was as follows: 10 mL concentrated HCl was added to 336.8 mL MilliQ water and constantly stirred at 25 °C. Then, 1.63 g aniline was added to the above solution and stirred in an ice bath at 150 rpm for 30 min. Afterward, 3.99 g ammonium persulfate was slowly added to the aniline solution and stirred in the ice bath for 24 h. Polyaniline was obtained by centrifugation at 8,000 rpm for 15 min. The oligomers and doped acid were removed by washing with MilliQ water and ethanol alternately several times, and the final pure product was dried in a vacuum drying oven at 60 °C for 12 h.

2.2. β-LG protein monomer purification

Ten grams of whey protein isolate (WPI, Fonterra, New Zealand) was dissolved in 90 mL ultra-pure water, and the pH of the solution was adjusted to 4.2 with concentrated hydrochloric acid. The conical flask containing the solution was incubated in a water bath oscillator at 60 °C (150 rpm) for 4 h until the solution became cloudy, then centrifuged (15 min at 8,000 rpm) to obtain a nearly transparent solution and white sediment. The supernatant was collected, and the centrifugation procedure was repeated more than twice. The supernatant was passed through a 0.45 μm microporous filter to further remove the remaining insoluble proteins. The obtained clear solution containing mainly β-LG protein monomers, residual salt, and sugar was transferred to a conical flask, freeze-dried, and stored at −20 °C to synthesize AFLs.

2.3. Synthesis of β-LG AFLs

An amyloid fibril solution with a mass fraction of 2 wt% was prepared using ultra-pure water with a pH of 2 and purified β-LG protein monomer. AFLs were heated in a 90 °C water bath with constant stirring for 5 h (120 rpm for the first 3 h and 170 rpm for the last 2 h). The synthesized β-LG AFLs were collected by centrifugation, immediately cooled using a water–ice mixture, and stored at 4 °C before use.

2.4. Formation of PPA gel beads

PVA solution with a mass fraction of 10 wt% was first prepared with MilliQ water and stirred in a water bath (90 °C) until completely dissolved. The PVA solution was cooled naturally to room temperature. Then, 0.2 g of PANI was dissolved in 20 mL AFL solution, and then added with 4 g of PVA solution. The mixture was stirred at 25 °C for 10 min (120 rpm), injected into the mold with a syringe, and freeze-thawed (−20 °C/25 °C) for three times. The final PPA composite beads were washed with water and transferred to a Petri dish for freeze-drying. The synthesis procedure can be referred to in Figure 1.

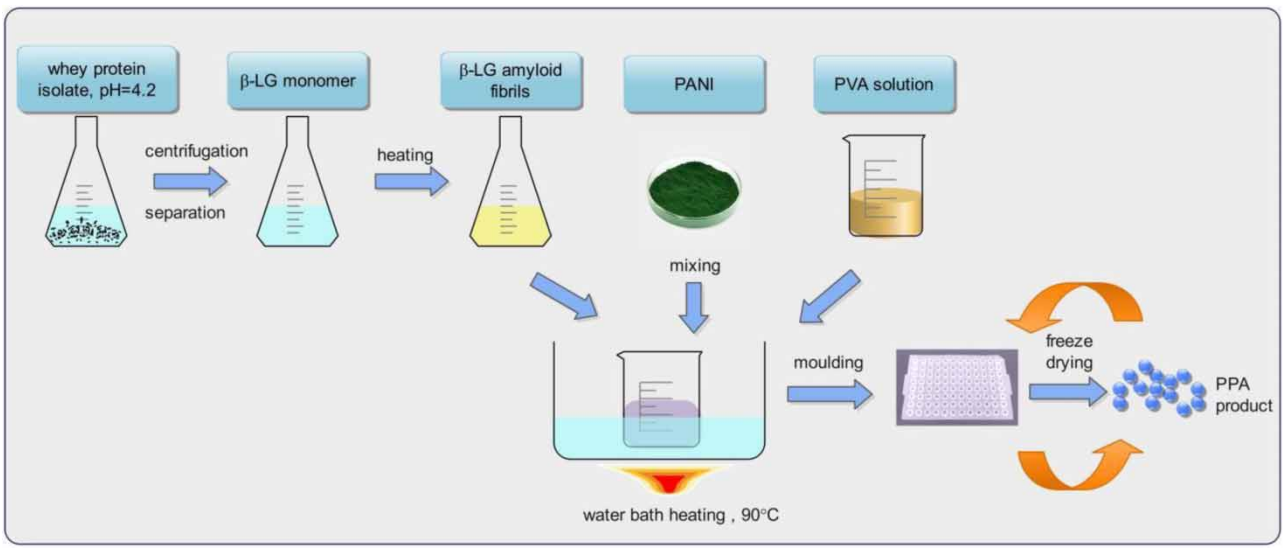

Figure 1 | Synthesis procedure of PPA composite beads.

2.5. Characterization

The morphology and elemental composition of PPA gel beads in water before and after Cr adsorption were characterized by scanning electron microscopy (SEM) coupled with an X-ray energy dispersion spectrometer (EDX) (Sigma 300, ZEISS, Germany). The PPA beads were crushed to powder and subjected to a zeta potential test at varying pHs 2, 4, 6, 8, and 10 on a Zeta sizer Nano-ZS90 (Malvern, UK). After the adsorption experiment, the beads were also powdered to analyze elemental valence states (Cr, C, and N) using X-ray photoelectron spectrometry (ESCALAB Xi + , Thermo Fisher Scientific, USA). X-ray powder diffraction (XRD) patterns of the materials before and after adsorption were obtained on a diffractometer (EMPYREAN, Holland) using Cu Kα radiation in a scanning range of 10–80° at a scanning rate of 2° min^{-1}. Jade 6.5 software (MDI) was used to analyze the typical mineral phases. Before and after adsorption, the materials were also subject to Fourier Transform Infrared Reflection (FTIR) (iN10, Thermo Fisher Scientific, USA) at the wavenumber of 600–4,000 cm^{-1}. The Brunauer–Emmett–Teller (BET) (ASAP 2460, Micromeritics, USA) method was used to obtain the specific surface area, pore size, and pore volume.

2.6. Batch adsorption experiment

The adsorption performance of PPA composite beads for Cr(VI) in water was studied by batch adsorption experiments. The adsorption kinetics experiment was carried out at the Cr(VI) concentration of 50 mg L^{-1} at pH = 3. The specific method was as follows: 40 mg of PPA beads was added into a conical flask containing 20 mL Cr(VI) solution with a concentration of 50 mg L^{-1}, and the flasks were oscillated in a constant temperature water bath oscillator (25 °C) at a speed of 150 rpm. Samples were intermittently taken out at different intervals (0–50 h) and then filtered through a 0.22 μm polyethersulfone (PES) membrane filter to determine the residual Cr(VI) concentration. There was no retention effect of Cr(VI) on the PES membrane based on our initial test. Three replicates were set for each sample. The residual Cr(VI) in the solution after adsorption equilibrium was determined by 1,5-dibenzoyl dihydrazine spectrophotometric method at 540 nm on a UV–Visible spectrophotometer (UV-2250, Shimadzu, Japan). The total Cr concentration in the solution was digested with nitric acid–peroxide (HNO_3–H_2O_2) and measured at 357.9 nm on an atomic absorption spectrometry (AAS) (AA700, PerkinElmer, USA). The Cr(III) content in the solution was calculated by subtracting the Cr(VI) content from the total Cr content. The limit of detection and limit of quantification of total Cr on AAS were 0.004 and 0.012 mg L^{-1}, respectively. The limit of detection and limit of quantification of Cr(VI) on UV–Vis were 0.068 and 0.21 mg L^{-1}, respectively.

An isothermal adsorption experiment was conducted to explore the influence of the initial concentration of the solution on adsorption. Specifically, 40 mg PPA beads were added into conical bottles containing 20 mL Cr(VI) solution with 5, 15, 25, 50, 100, 250, and 400 mg L^{-1} concentration gradients, respectively. Samples were oscillated in a constant temperature water bath oscillator (25 °C) at 150 rpm for 48 h. The samples were then treated, and Cr(VI) concentration was examined in the same way as described above. The removal efficiency (W) and adsorption capacity (Q_e) of Cr(VI) were calculated according to the following equations (Gao & Xia 2011; Kapoor *et al.* 2022):

$$W(\%) = \frac{C_0 - C_e}{C_0} \times 100 \tag{1}$$

$$Q_e = \frac{(C_0 - C_e) \times V}{m} \tag{2}$$

where W (%) is the removal rate of Cr(VI); Q_e (mg g^{-1}) is the removal capacity of Cr(VI); C_o and C_e (mg L^{-1}) represent the initial and equilibrium concentration of Cr(VI), respectively; m (g) represents the mass of the adsorbent, and V (L) represents the volume of the solution.

In addition, the effect of temperature on the adsorption of PPA was determined at 25, 35, and 45 °C (Cr(VI) concentration of 50 mg L^{-1}, pH = 3). The standard free energy change (ΔG), standard enthalpy change (ΔH), standard entropy change (ΔS), and other thermodynamic parameters are calculated according to the following formulae (Peng *et al.* 2009; Wang *et al.* 2021):

$$\Delta G = -RT \ln \frac{Q_e}{C_e} \tag{3}$$

$$\Delta G = \Delta H - T\Delta S \tag{4}$$

where ΔG (kJ mol^{-1}) is the change of free energy of Gipps; R (8.314 J mol^{-1} K^{-1}) is the ideal gas constant; T (K) is the absolute temperature; ΔH (kJ mol^{-1}) is adsorption enthalpy; and ΔS (J mol^{-1} K^{-1}) is the adsorption entropy change.

2.7. Models

The adsorption kinetics of Cr(VI) onto the PPA beads were analyzed by fitting the data with the pseudo-first-order model, the pseudo-second-order model, and the Weber–Morris model (Liu *et al.* 2022; Wu *et al.* 2022):

$$\text{Pseudo-first-order model:} \quad Q_t = Q_e - Q_e e^{(-k_1 t)} \tag{5}$$

$$\text{Pseudo-second-order model:} \quad Q_t = \frac{k_2 Q_e^2 t}{1 + k_2 Q_e t} \tag{6}$$

where Q_t and Q_e (mg g^{-1}) are the material's adsorption capacity at time t and equilibrium, respectively; t (min) is the varied vibrating time; the k_1 (min^{-1}) and k_2 (g mg^{-1} min^{-1}) is the adsorption rate constant of the pseudo-first-order model and the pseudo-second-order model, respectively.

The isothermal adsorption was analyzed by Langmuir model, Freundlich model, and Redlich–Peterson model (Quan *et al.* 2014; Zhang *et al.* 2018; Wang *et al.* 2020):

$$\text{Langmuir model:} \quad Q_e = \frac{K_L Q_m C_e}{1 + K_L C_e} \tag{7}$$

$$\text{Freundlich model:} \quad Q_e = K_F C_e^{\frac{1}{n}} \tag{8}$$

$$\text{Redlich-Peterson model:} \quad Q_e = \frac{K_R C_e}{1 + \alpha C_e^{\beta}} \tag{9}$$

where Q_e (mg g^{-1}) is the adsorption capacity at equilibrium time; Q_m (mg g^{-1}) is the maximum removal capacity; C_e and C_m (mg L^{-1}) represent the equilibrium and the maximum concentration, respectively; K_L (L mg^{-1}), K_F (mg g^{-1}·(mg L^{-1})$^{-1/n}$), and K_R (L g^{-1}) are the Langmuir, Freundlich, and Redlich–Peterson (R-P) isotherm constants, respectively; n is the Freundlich constant indicates the adsorption strength; α (L mg^{-1}) is the R-P isotherm constant related to binding site affinity, and β is the R-P isotherm exponent related to adsorption strength.

3. RESULTS AND DISCUSSION

3.1. Characterization and properties of PPA beads

The prepared PPA beads using HCl as doping acid were dark green spheres with a diameter of 6 mm (Figure 2(a)), indicating that polyaniline existed as emerald imine in the gel beads (Wang *et al.* 2009). The PPA beads had toughness and resilience, and it can restore the shape when squeezed with fingers. The PPA beads were subject to a simple adsorption test (50 mg L^{-1} Cr(VI), pH 3, 3 h, PPA dosage of 1 g L^{-1}) to test its adsorption ability, and the changes in morphology and elemental composition were recorded using SEM-EDX. The pilot adsorption test revealed a 97% removal efficiency, with removal outcome

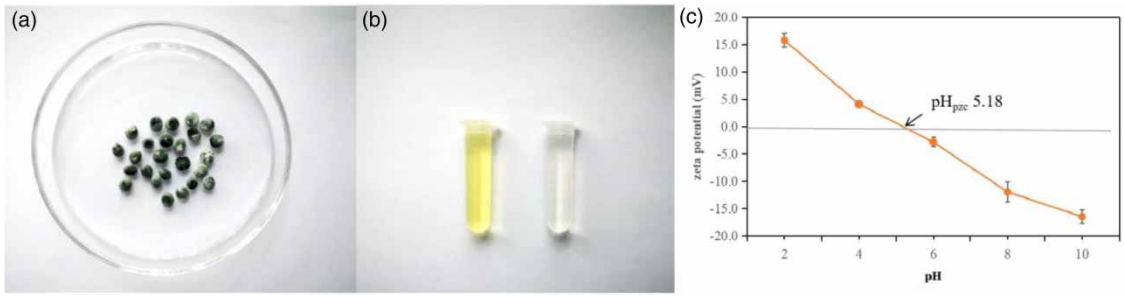

Figure 2 | (a) The spherical morphology of PPA beads, (b) the Cr(VI) solution (50 mg L^{-1}) before and after PPA treatment, and (c) the zeta potential of PPA at varying pHs.

observable from the color change of the Cr(VI) solution before and after the reaction (Figure 2(b)). In addition, the PPA had a positive surface charge at $pH_{pzc} < 5.18$ but a negative surface charge at $pH_{pzc} > 5.18$ (Figure 2(c)), suggesting that the acidic environment may be more conducive to Cr(VI) adsorption as a result of electrostatic attraction. The SEM profile showed that the inside of the PPA beads before adsorption had a three-dimensional porous structure (Figure 3(a) and 3(b)), and the rough and wrinkled surfaces that made up the pores of the material can be observed, which was conducive to Cr(VI) penetration. The BET surface area and average pore size were calculated to be 14 $m^2 g^{-1}$ and 19.12 nm, respectively (Table 1), indicating the mesoporous structure of PPA. After adsorption, it can be observed that particle microspheres were formed (Figure 3(d) and 3(e)), and its BET surface area and average pore size were reduced to 14 $m^2 g^{-1}$ and 16.68 nm, respectively. The pore volume after adsorption was also slightly decreased as compared to that before adsorption. These changes could be due to the adsorption of a large number of Cr ions and/or Cr-complexes outside and inside the gel sphere. Elements C, N, O, and Cr in the PPA were analyzed before and after Cr(VI) adsorption in solution (Figure 3(c) and 3(f)). According to the EDX diagram, a new peak of about 5.5 keV belonging to Cr appeared after the adsorption, with an atomic percentage of 38.64%. Meanwhile, the contents of other elements all decreased to varying degrees (C: 40.43 to 23.02%, N: 17.08 to 10.32%, and O: 41.63 to 28.03%).

3.2. Adsorption kinetics

The adsorption kinetics curve parameters fitted with the pseudo-first and pseudo-second kinetics models are summarized in Table 2, and the fitted lines are shown in Figure 4(a). The adsorption rate was quick in the initial 8 h of the adsorption. Still, the adsorption rate gradually slowed down with time approaching 12 h and after. After 48 h, the adsorption capacity was calculated to be 24.2 mg g^{-1} with a removal rate of 97%. According to the correlation coefficient, the R^2 value of the pseudo-second-order kinetics model (0.9874) was higher than that of the pseudo-first-order kinetics model (0.7090), indicating that the adsorption behavior of Cr(VI) onto the polyaniline/polyvinyl alcohol/sodium alginate (PPS) composite beads was better described by the pseudo-second-order kinetics. In addition, the Cr(III) concentrations in the supernatants after adsorption at different intervals were all below the detection limit. Thus, the adsorption of Cr(VI) and its subsequent conversion of Cr(III) could both occur on the material, and no Cr(III) was mobilized and released from the PPA material.

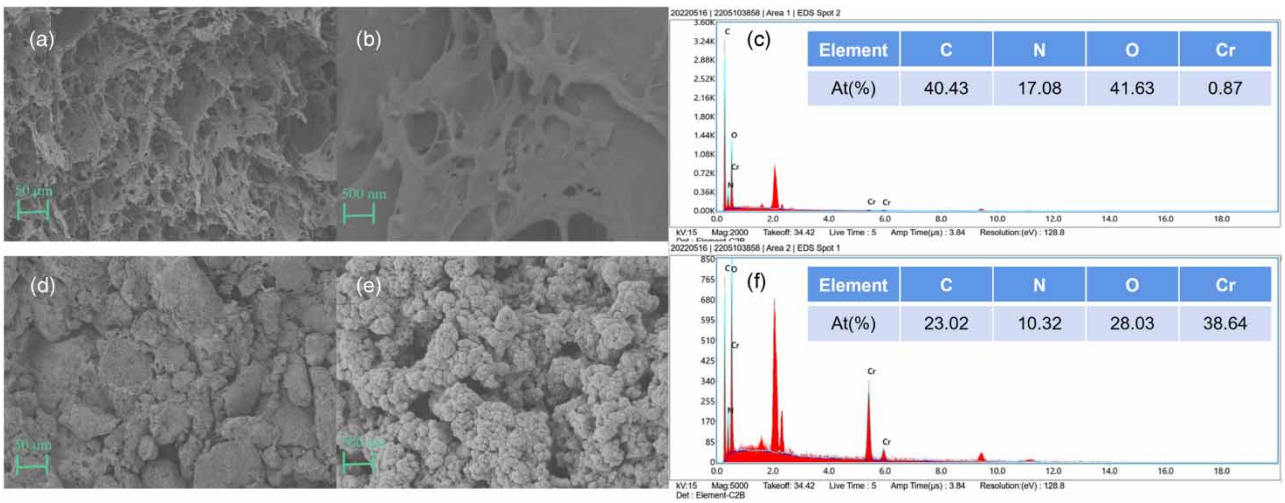

Figure 3 | SEM image of PPA before (a, b) and after (d, e) adsorption; and EDX analysis of C, N, O, and Cr before (c) and after adsorption (f).

Table 1 | The specific surface area, pore volume, and pore size of PPA before and after adsorption

Samples	BET surface area ($m^2 g^{-1}$)	Pore volume ($cm^3 g^{-1}$)	Average pore size (nm)
PPA before adsorption	14	0.09788	19.12
PPA after adsorption	12	0.09054	16.68

Table 2 | Adsorption kinetics and isothermal parameters

Adsorption models	Parameter	Value
Adsorption kinetics		
Pseudo-first-order	Q_e (mg g^{-1})	23.13
	k_1 (L min^{-1})	0.0135
	R^2	0.7090
Pseudo-second-order	Q_e (mg g^{-1})	24.64
	k_2 (g mg^{-1} min^{-1})	0.0008
	R^2	0.9874
Adsorption isotherms		
Langmuir	Q_m (mg g^{-1})	51.54
	K_L (L mg^{-1})	0.2327
	R_L	0.0127
	R^2	0.9171
Freundlich	K_F (mg (mg L^{-1})$^{-1/n}$)	28.43
	$1/n$	0.1146
	R^2	0.8245
Redlich–Peterson	K_R (L g^{-1})	12.00
	α (L mg^{-1})	0.2327
	β	1
	R^2	0.9915

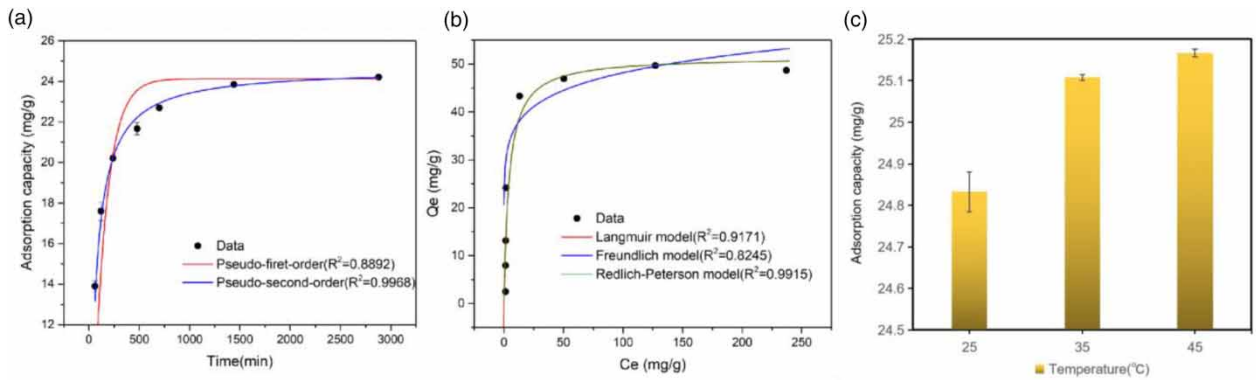

Figure 4 | Cr(VI) adsorption on PPA composite beads: (a) adsorption kinetics, (b) adsorption isotherms, and (c) adsorption capacity affected by temperature change.

3.3. Adsorption isotherms

The isothermal adsorption results showed that the removal ability of PPA composite beads for Cr(VI) in water increased with the initial concentration of a solution (Figure 4(b)). The adsorption increased rapidly when the concentration of Cr(VI) increased from 5 to 100 mg L^{-1}. The adsorption tended to reach the plateau when the concentration reached 150 mg L^{-1}. At the low concentrations, the adsorption sites on the PPA beads were sufficient to remove Cr(VI) continuously. With increasing concentrations, the adsorption amount ceased to increase and reached saturation due to the limited number of adsorption sites. The Langmuir, Freundlich, and R-P models were used to analyze the isothermal adsorption process, and the parameters obtained are shown in Table 2. The correlation coefficients (R^2) of the Langmuir, Freundlich, and R-P models were 0.9171, 0.8245, and 0.9915, respectively. Therefore, the adsorption process of Cr(VI) on PPA beads can be described better by the R-P model because it was the closest to 1. Noteworthy, the value of β is the R-P constant related to the adsorption strength, and its value is between 0 and 1 and cannot be greater than 1 (Tshemese *et al.* 2021). When the value of β is 1, the R-P model equation can be simplified to the Langmuir model equation (Yang *et al.* 2020). In this study, the β value of the R-P model was 1, suggesting that the adsorption was monolayer adsorption with homogeneous surface reaction sites. The maximum

adsorption capacity obtained by the Langmuir isothermal model was 51.54 mg g^{-1}. Since the value of R_L and the value of $1/n$ were between 0 and 1, the adsorption of Cr(VI) by PPA composite beads was favorable (Yang *et al.* 2020). Table 3 lists the adsorption capacity of different polyaniline composite adsorbents for Cr(VI). Compared with other polyaniline-related composites, the size of PPA was the largest among them, but the adsorption capacity of PPA for Cr(VI) was in the upper middle range. Although the adsorption capacity of PPA was lower than the PPS product made of PANI, PVA, and sodium alginate in our previous study (Li *et al.* 2022), the lower maximum Cr(VI) concentration (400 mg L^{-1}) in the current study may contribute to the decrease. Noteworthy, the size of PPA was about two times bigger than that of PPS; there is still a likelihood of increasing the PPA's adsorption capacity by size adjustment. Considering the easy aggregation of nano-polyaniline adsorbent when applied in the water environment, the PPA beads have a high potential for water purification because of their excellent separation performance. The large particle size will facilitate recycling and recovery and not cause secondary pollution.

3.4. Adsorption thermodynamics

The adsorption capacity of Cr(VI) on PPS material generally followed an increasing trend with the increase in temperature (Figure 4(c)). The thermodynamic parameters, including standard free energy change (ΔG), standard enthalpy change (ΔH), and standard entropy change (ΔS) are summarized in Table 4. The ΔG values were negative, indicating that the adsorption of Cr(VI) by PPA was spontaneous. The ΔH of 9.62 kJ $mol^{-1} > 0$ suggested that the adsorption was an endothermic process. Therefore, increasing the temperature is conducive to promoting the adsorption efficiency of PPA for Cr(VI). In addition, the ΔS value was above zero, suggesting that the adsorption of Cr(VI) onto PPA was an entropy increase process, where the chaos of the solid–liquid interface will increase during the adsorption.

3.5. Adsorption mechanisms

Figure 5 shows the characteristic binding energies of Cr 2*p*, C 1*s*, O 1*s*, and N 1*s* before and after the adsorption reaction. From the high-resolution spectrogram of Cr 2*p*, it can be seen that Cr 2*p*1/2 (586.9 eV) and Cr 2*p*3/2 (577.1 eV) all belong to Cr(III) (Zhou *et al.* 2017; Hamza *et al.* 2020). The presence of Cr(III) characteristic peaks proved that the Cr(VI) adsorbed by PPA was almost completely reduced to Cr(III). The C 1*s* (Figure 5(b)) peaks at 284.6, 285.4, 286.1, and 288.4 eV belong to C–C/C–H, C–N, C–OH, and C = O (Rozada *et al.* 2005; Shang *et al.* 2021), respectively. After adsorption, the peak area of C = O slightly shifted to a higher energy position (288.7 eV) (Guo *et al.* 2016) and increased from 1.4 to 3.9%, and the percentage of C–O reduced from 28.9 to 13.0%. It indicated that redox reactions occurred on the PPA; that is, Cr(VI) adsorbed on PPA may be reduced to Cr(III) by an electron donor C–O, and at the same time, C–O was oxidized to C = O (Li *et al.* 2022). By observing the XPS spectra of O 1*s* (Figure 5(c)), it can be found that the characteristic peaks of 531.3 and 532.1 eV before the reaction corresponds to C = O and C–OH (Arputharaj *et al.* 2021), respectively. After adsorption, the peak

Table 3 | Adsorption capacities of various polyaniline-based composites

Material	Experimental condition	Morphology	Adsorption capacity	Ref.
PANI@PS beads	pH = 6.0, T = 25 °C	Ball shape, 0.4–0.6 mm	12.15 mg g^{-1}	Ding *et al.* (2018)
PANI/ECs	pH = 1.0	Irregular, 500 nm	38.76 mg g^{-1}	Qiu *et al.* (2014)
HA@PANI	pH = 5.07, T = 25 °C	Nanotube, width 30–70 nm	62.9 mg g^{-1}	Zhou *et al.* (2017)
PPS	C_{max} = 800 mg g^{-1}, pH = 3.0, T = 25 °C	Ball shape, 2–3 mm	83.1 mg g^{-1}	Li *et al.* (2022)
PANI/MWCNT nanotubes	T = 35 °C	Nanotube, width 50 nm	36.76 mg g^{-1}	Wang *et al.* (2015)
PPA composite beads	C_{max} = 400 mg g^{-1}, pH = 3.0, T = 25 °C	Ball shape, 5–6 mm	51.5 mg g^{-1}	This study

Table 4 | Thermodynamics parameters of Cr(VI) adsorption onto PPA

Temperature (°C)	Q_e (mg g^{-1})	$\triangle G$ (kJ mol^{-1})	$\triangle H$ (kJ mol^{-1})	$\triangle S$ (J mol^{-1} K^{-1})
25	24.883	− 5.473		
35	25.108	− 6.141	9.620	50.800
45	25.167	− 6.489		

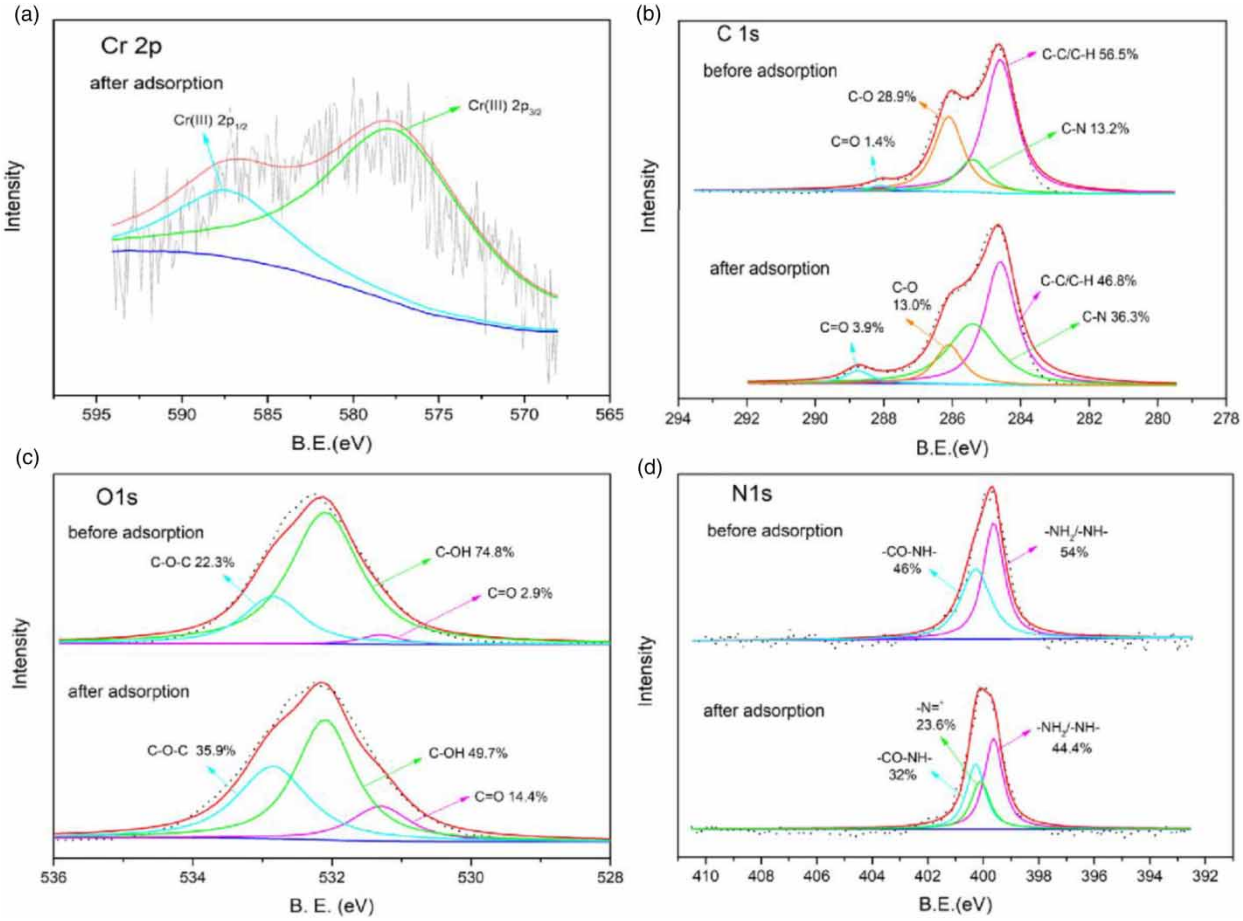

Figure 5 | The XPS spectrum of (a) Cr 2*p*, (b) C 1*s*, (c) O 1*s*, and (d) N 1*s* on the PPA material.

area of C = O increased from 2.9 to 14.4%, and the peak area of C–OH decreased from 74.8 to 49.7%. It further supports the above statement that C–OH may be used as an electron donor to reduce Cr(VI) to Cr(III) and form C = O bonds. In the XPS spectrum of N 1*s* (Figure 5(d)), the characteristic peaks at 399.63, 400.27, and 400.1 eV correspond to –NH_2/–NH–, –CO–NH–, and –N = $^+$ (Ding *et al.* 2018; Geng *et al.* 2019; Li *et al.* 2022), respectively. By comparing the changes of N 1*s* spectra before and after the reaction, it can be found that the relative intensity of the characteristic peak belonging to –NH– decreased after the adsorption reaction, while the appearance of –N = $^+$ would benefit the electrostatic attraction of Cr(VI) toward the material and also proved the –NH–/–N= redox reaction took place in the system.

The FTIR and XRD patterns of PPA before and after the adsorption reaction were also analyzed and shown in Figure 6. For the PPA before the adsorption process (Figure 6(a)), the peak at 3,265 cm^{-1} was generated by tensile vibrations of O–H and N–H (Geng *et al.* 2019). The absorption band at 2,944 cm^{-1} was caused by the C–H bond (Hu *et al.* 2020). The 1,630 and 1,309 cm^{-1} peaks were assigned to the stretching vibration of the amide and C–N, respectively (Yan *et al.* 2017), and the peak at 1,094 cm^{-1} belonged to C–O–C (Yan *et al.* 2017). After adsorption, there was an appearance of –COOH at 1,419 cm^{-1} (Yan *et al.* 2017). Meanwhile, the reduced intensity of O–H and N–H at 3,267 cm^{-1} and the red-shift of amide and C–N peaks all suggested that the oxygen and nitrogen-containing groups were involved in the Cr(VI) adsorption and reduction process. The XRD analysis showed that the major chemicals existing in the PPA before adsorption were mainly hydrogen urea nitrate ($OC(NH_2)_2H)NO_3$ and ammonium thiosulfate ($(NH_4)_2S_2O_3$) (Figure 6(b)). After adsorption, the diffraction peaks lack a fine spectral peak structure with a low signal-to-noise ratio, indicating the presence of impurities and various amorphous products. The presence of $(OC(NH_2)_2H)NO_3$ was not found after adsorption. Typical diffraction peaks belonging to chromium hydroxide hydrate ($Cr(OH)_3{\cdot}3H_2O$) (e.g., 19.4°, 60.5°) and chromium oxides (Cr_2O_3) (e.g., 65.4°, 67.3°) appeared, which also verified the production of Cr(III) compounds after adsorption.

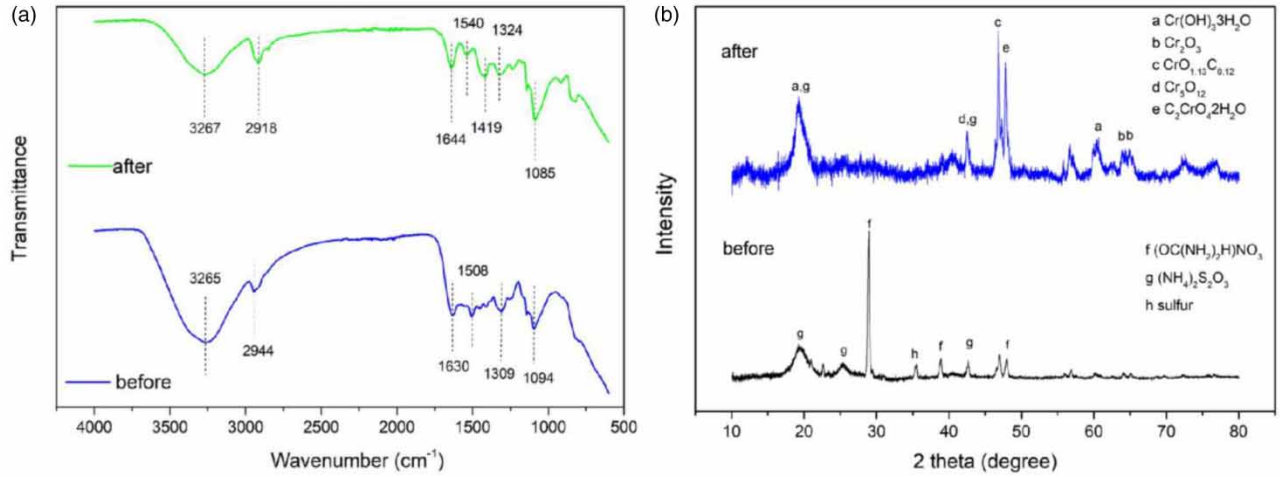

Figure 6 | (a) FTIR and (b) XRD graphs of the PPA material before and after adsorption.

Therefore, the inner mechanisms of the adsorption process can be described as follows: when the Cr(VI) anions were in contact with the PPA beads, the positive surface charge electrostatically attracted the Cr(VI), and the porous structure allowed the penetration of Cr(VI) into the material. The abundant –NH– groups and C–OH groups underwent redox reactions when reacting with Cr(VI), leading to the generation of Cr(III) and the corresponding –N= and C = O groups. Besides, the undetectable Cr(III) content in the supernatant after adsorption suggested that the Cr(III) reduced from Cr(VI) was well stabilized in the PPA beads, possibly due to the complexation occurring between Cr(III) and C–OH groups (Figure 7).

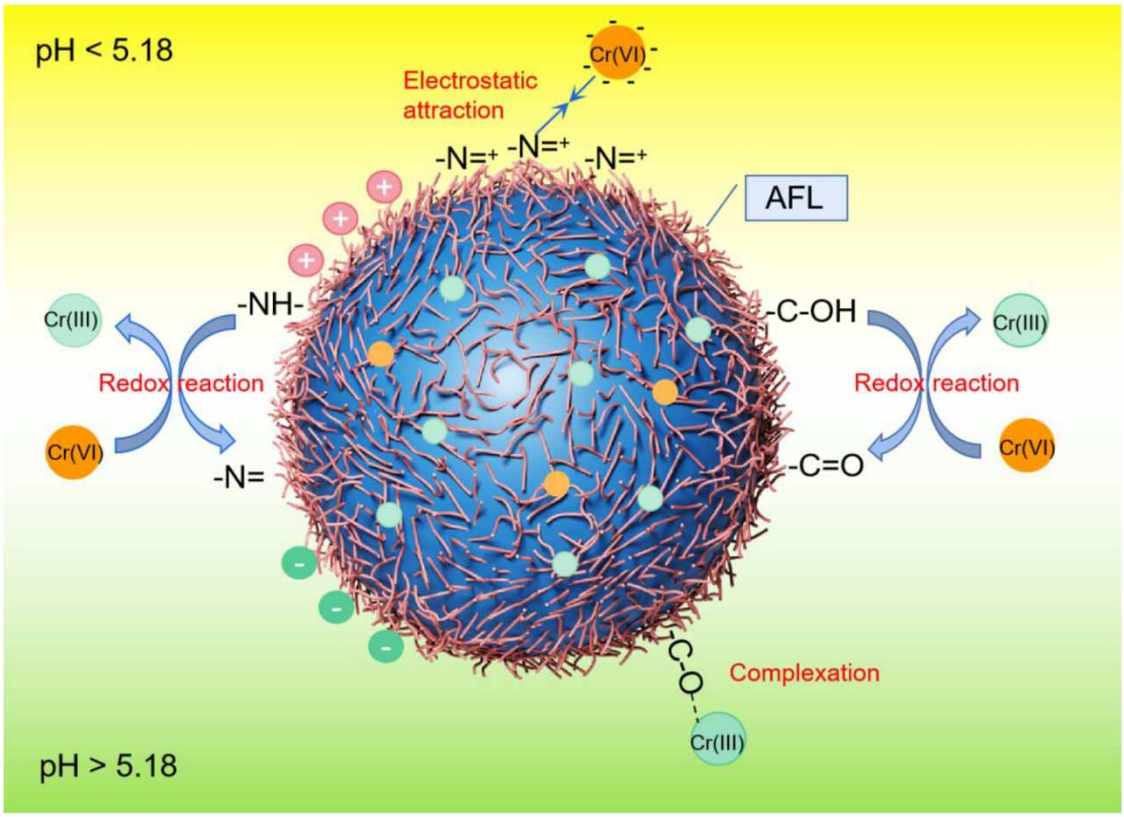

Figure 7 | Possible mechanisms involved in Cr adsorption by the PPA beads.

4. CONCLUSION

In this study, we synthesized a bulk adsorbent PPA with a combination of polyaniline, polyvinyl alcohol, and amyloid fibril. The as-formed material exhibited good adsorption capacity for Cr with Q_m of 51.5 mg g^{-1}. The adsorption capacity was comparable to or even better than some PANI-based nanomaterials. The adsorption process was mainly pseudo-second-order controlling kinetics and followed Langmuir adsorption isotherm, suggesting chemical reactions governed the adsorption chiefly. The XPS analysis further proved the above result, where the redox reactions happened between –NH–, C–OH groups, and Cr(VI) anions caused the formation of Cr(III), which was further stabilized within the PPA beads through complexation. The synthesis and use of PPA beads provide a new way of using bulk-size material for heavy metal remediation, especially in soil remediation, where the bulk material can be easily collected and regenerated. This study provided the initial data of using PPA for Cr remediation. Future research is needed in the aspects of influencing factors, material's reusability, material's stability, etc., to evaluate the potential ability of this material in the broader application.

ACKNOWLEDGEMENTS

The study was supported by the Natural Science Foundation of Chongqing (CSTB2022NSCQ-MSX0391), the National Natural Science Foundation of China (No. 52370166), the Natural Science Foundation of Hunan Province (No. 2023JJ30126), and the Natural Science Foundation of Changsha City (No. kq2208020).

AUTHOR CONTRIBUTIONS

J.W.: original draft, methodology, funding acquisition; Y.Z.: data curation, experiment; Y.D.: experiment, data curation.

DATA AVAILABILITY STATEMENT

All relevant data are included in the paper or its Supplementary Information.

CONFLICT OF INTEREST

The authors declare there is no conflict.

REFERENCES

Anantha-Iyengar, G., Shanmugasundaram, K., Nallal, M., Lee, K.-P., Whitcombe, M. J., Lakshmi, D. & Sai-Anand, G. 2019 Functionalized conjugated polymers for sensing and molecular imprinting applications. *Prog. Polym. Sci.* **88**, 1–129.

Arputharaj, E., Krishna Kumar, A. S., Tseng, W. L., Jiang, S. J., Huang, Y. L. & Dahms, H. U. 2021 Self-assembly of poly(ethyleneimine)-modified g-C_3N_4 nanosheets with lysozyme fibrils for chromium detoxification. *Langmuir* **37**, 7147–7155.

Chen, X., Dai, Y., Fan, J., Xu, X. & Cao, X. 2021 Application of iron-biochar composite in topsoil for simultaneous remediation of chromium-contaminated soil and groundwater: Immobilization mechanism and long-term stability. *J. Hazard. Mater.* **405**, 124226.

Chen, D., Du, X., Chen, K., Liu, G., Jin, X., Song, C., He, F. & Huang, Q. 2022 Efficient removal of aqueous Cr(VI) with ferrous sulfide/N-doped biochar composites: Facile, in-situ preparation and Cr(VI) uptake performance and mechanism. *Sci. Total Environ.* **837**, 155791.

Chrysochoou, M. & Reeves, K. 2017 Reduction of hexavalent chromium by green tea polyphenols and green tea nano zero-valent iron (GT-NZVI). *Bull. Environ. Contam. Toxicol.* **98**, 353–358.

Cui, R., Xiao, Y., Li, C., Han, Y., Lv, G. & Zhang, Z. 2020 Polyaniline/reduced graphene oxide foams as metal-free cathodes for stable lithium–oxygen batteries. *Nanotechnology* **31**, 445402.

Derakhshankhah, H., Mohammad-Rezaei, R., Massoumi, B., Abbasian, M., Rezaei, A., Samadian, H. & Jaymand, M. 2020 Conducting polymer-based electrically conductive adhesive materials: Design, fabrication, properties, and applications. *J. Mater. Sci. Mater. Electron.* **31**, 10947–10961.

Ding, J., Pu, L., Wang, Y., Wu, B., Yu, A., Zhang, X., Pan, B., Zhang, Q. & Gao, G. 2018 Adsorption and reduction of Cr(VI) together with Cr(III) sequestration by polyaniline confined in pores of polystyrene beads. *Environ. Sci. Technol.* **52**, 12602–12611.

Dong, H., Zhang, L., Shao, P., Hu, Z., Yao, Z., Xiao, Q., Li, D., Li, M., Yang, L., Luo, S. & Luo, X. 2023 A metal-organic framework surrounded with conjugate acid-base pairs for the efficient capture of Cr(VI) via hydrogen bonding over a wide pH range. *J. Hazard. Mater.* **441**, 129945.

Farooqi, Z. H., Akram, M. W., Begum, R., Wu, W. & Irfan, A. 2021 Inorganic nanoparticles for reduction of hexavalent chromium: Physicochemical aspects. *J. Hazard. Mater.* **402**, 123535.

Gao, Y. & Xia, J. 2011 Chromium contamination accident in China: Viewing environment policy of China. *Environ. Sci. Technol.* **45**, 8605–8606.

Geng, J., Yin, Y., Liang, Q., Zhu, Z. & Luo, H. 2019 Polyethyleneimine cross-linked graphene oxide for removing hazardous hexavalent chromium: Adsorption performance and mechanism. *Chem. Eng. J.* **361**, 1497–1510.

Godiya, C. B., Sayed, S. M., Xiao, Y. & Lu, X. 2020 Highly porous egg white/polyethyleneimine hydrogel for rapid removal of heavy metal ions and catalysis in wastewater. *React. Funct. Polym.* **149**, 104509.

Guo, X., Fei, G. T., Su, H. & De Zhang, L. 2011 High-performance and reproducible polyaniline nanowire/tubes for removal of Cr(VI) in aqueous solution. *J. Phys. Chem. C* **115**, 1608–1613.

Guo, Z., Xiao, Z., Ren, G., Xiao, G., Zhu, Y., Dai, L. & Jiang, L. 2016 Natural tea-leaf-derived, ternary-doped 3D porous carbon as a high-performance electrocatalyst for the oxygen reduction reaction. *Nano Res.* **9**, 1244–1255.

Hamza, M. F., Lu, S., Salih, K. A. M., Mira, H., Dhmees, A. S., Fujita, T., Wei, Y., Vincent, T. & Guibal, E. 2020 As(V) sorption from aqueous solutions using quaternized algal/polyethyleneimine composite beads. *Sci. Total Environ.* **719**, 137396.

Han, Y., Cao, Y., Bolisetty, S., Tian, T., Handschin, S., Lu, C. & Mezzenga, R. 2020 Amyloid fibril-templated high-performance conductive aerogels with sensing properties. *Small* **16**, 2004932.

Hu, X., Wen, J., Zhang, H., Wang, Q., Yan, C. & Xing, L. 2020 Can epicatechin gallate increase Cr(VI) adsorption and reduction on ZIF-8? *Chem. Eng. J.* **391**, 123501.

Kapoor, R. T., Bani Mfarrej, M. F., Alam, P., Rinklebe, J. & Ahmad, P. 2022 Accumulation of chromium in plants and its repercussion in animals and humans. *Environ. Pollut.* **301**, 119044.

Kong, Q., Wei, J., Hu, Y. & Wei, C. 2019 Fabrication of terminal amino hyperbranched polymer modified graphene oxide and its prominent adsorption performance towards Cr(VI). *J. Hazard. Mater.* **363**, 161–169.

Leung, W. H., Zou, L., Lo, W. H. & Chan, P. H. 2013 An amyloid-fibril-based colorimetric nanosensor for rapid and sensitive chromium(VI) detection. *ChemPlusChem* **78**, 1440–1445.

Li, J., Li, M., Wang, S., Yang, X., Liu, F. & Liu, X. 2020 Key role of pore size in Cr(VI) removal by the composites of 3-dimensional mesoporous silica nanospheres wrapped with polyaniline. *Sci. Total Environ.* **729**, 139009.

Li, Y., Wen, J., Xue, Z., Yin, X., Yuan, L. & Yang, C. 2022 Removal of Cr(VI) by polyaniline embedded polyvinyl alcohol/sodium alginate beads – extension from water treatment to soil remediation. *J. Hazard. Mater.* **426**, 127809.

Liu, B. & Huang, Y. 2011 Polyethyleneimine modified eggshell membrane as a novel biosorbent for adsorption and detoxification of Cr(VI) from water. *J. Mater. Chem.* **21**, 17413–17418.

Liu, X., Zhang, S., Zhang, X., Guo, H., Lou, Z., Zhang, W. & Chen, Z. 2022 Cr(VI) immobilization in soil using lignin hydrogel supported NZVI: Immobilization mechanisms and long-term simulation. *Chemosphere* **305**, 135393.

Lv, X., Jiang, G., Xue, X., Wu, D., Sheng, T., Sun, C. & Xu, X. 2013 Fe^0-Fe_3O_4 nanocomposites embedded polyvinyl alcohol/sodium alginate beads for chromium (VI) removal. *J. Hazard. Mater.* **262**, 748–758.

Mahanta, D., Madras, G., Radhakrishnan, S. & Patil, S. 2009 Adsorption and desorption kinetics of anionic dyes on doped polyaniline. *J. Phys. Chem. B* **113**, 2293–2299.

Peng, B., Huang, S., Yang, Z., Chai, L., Xu, Y. & Su, C. 2009 Inhibitory effect of Cr(VI) on activities of soil enzymes. *J. Cent. South Univ. Technol.* **16**, 594–598.

Perumal, A., Kanumuri, R., Rayala, S. K. & Nallaiyan, R. 2020 Fabrication of bioactive corrosion-resistant polyaniline/TiO_2 nanotubes nanocomposite and their application in orthopedics. *J. Mater. Sci.* **55**, 15602–15620.

Peydayesh, M., Bolisetty, S., Mohammadi, T. & Mezzenga, R. 2019 Assessing the binding performance of amyloid–carbon membranes toward heavy metal ions. *Langmuir* **35**, 4161–4170.

Peydayesh, M., Suter, M. K., Bolisetty, S., Boulos, S., Handschin, S., Nyström, L. & Mezzenga, R. 2020 Amyloid fibrils aerogel for sustainable removal of organic contaminants from water. *Adv. Mater.* **32**, 1907932.

Qiu, B., Xu, C., Sun, D., Yi, H., Guo, J., Zhang, X., Qu, H., Guerrero, M., Wang, X., Noel, N., Luo, Z., Guo, Z. & Wei, S. 2014 Polyaniline coated ethyl cellulose with improved hexavalent chromium removal. *ACS Sustainable Chem. Eng.* **2**, 2070–2080.

Quan, G., Zhang, J., Guo, J. & Lan, Y. 2014 Removal of Cr(VI) from aqueous solution by nanoscale zero-valent iron grafted on acid-activated attapulgite. *Water Air Soil Pollut.* **225**, 1979.

Ramírez-Rodríguez, L. C., Díaz Barrera, L. E., Quintanilla-Carvajal, M. X., Mendoza-Castillo, D. I., Bonilla-Petriciolet, A. & Jiménez-Junca, C. 2020 Preparation of a hybrid membrane from whey protein fibrils and activated carbon to remove mercury and chromium from water. *Membranes* **10**, 386.

Rozada, F., Otero, M., Parra, J. B., Morán, A. & García, A. I. 2005 Producing adsorbents from sewage sludge and discarded tyres: Characterization and utilization for the removal of pollutants from water. *Chem. Eng. J.* **114**, 161–169.

Sangeetha, K., Angelin Vinodhini, P., Sudha, P. N., Alsharani Faleh, A. & Sukumaran, A. 2019 Novel chitosan based thin sheet nanofiltration membrane for rejection of heavy metal chromium. *Int. J. Biol. Macromol.* **132**, 939–953.

Shang, J., Guo, Y., He, D., Qu, W., Tang, Y., Zhou, L. & Zhu, R. 2021 A novel graphene oxide-dicationic ionic liquid composite for Cr(VI) adsorption from aqueous solutions. *J. Hazard. Mater.* **416**, 125706.

Shi, T., Yang, D., Yang, H., Ye, J. & Cheng, Q. 2017 Preparation of chitosan crosslinked modified silicon material and its adsorption capability for chromium(VI). *Appl. Clay Sci.* **142**, 100–108.

Song, W., Shi, T., Yang, D., Ye, J., Zhou, Y. & Feng, Y. 2015 Pretreatment effects on the sorption of Cr(VI) onto surfactant-modified zeolite: Mechanism analysis. *J. Environ. Manage.* **162**, 96–101.

Tshemese, S. J., Mhike, W. & Tichapondwa, S. M. 2021 Adsorption of phenol and chromium (VI) from aqueous solution using exfoliated graphite: Equilibrium, kinetics and thermodynamic studies. *Arab. J. Chem.* **14**, 103160.

Wang, J., Deng, B., Chen, H., Wang, X. & Zheng, J. 2009 Removal of aqueous Hg(II) by polyaniline: Sorption characteristics and mechanisms. *Environ. Sci. Technol.* **43**, 5223–5228.

Wang, J., Zhang, K. & Zhao, L. 2014 Sono-assisted synthesis of nanostructured polyaniline for adsorption of aqueous Cr(VI): Effect of protonic acids. *Chem. Eng. J.* **239**, 123–131.

Wang, J. H., Yin, X. L., Tang, W. & Ma, H. R. 2015 Combined adsorption and reduction of Cr(VI) from aqueous solution on polyaniline/multiwalled carbon nanotubes composite. *Korean J. Chem. Eng.* **32**, 1889–1895.

Wang, K., Chen, P., Nie, W., Xu, Y. & Zhou, Y. 2019 Improved photocatalytic reduction of Cr(VI) by molybdenum disulfide modified with conjugated polyvinyl alcohol. *Chem. Eng. J.* **359**, 1205–1214.

Wang, J., Ma, R., Li, L., Gu, P. & Wang, X. 2020 Chitosan modified molybdenum disulfide composites as adsorbents for the simultaneous removal of U(VI), Eu(III), and Cr(VI) from aqueous solutions. *Cellulose* **27**, 1635–1648.

Wang, Q., Wen, J., Hu, X., Xing, L. & Yan, C. 2021 Immobilization of Cr(VI) contaminated soil using green-tea impregnated attapulgite. *J. Cleaner Prod.* **278**, 123967.

Wu, Q., Mo, W., Liu, J., Peng, S., Li, Q. & Wan, R. 2022 Remediation of high-concentration Cr(VI)-contaminated soils with $FeSO_4$ combined with biostimulation: Cr(VI) transformation and stabilization. *J. Hazard. Mater. Adv.* **8**, 100161.

Yan, Y., An, Q., Xiao, Z., Zheng, W. & Zhai, S. 2017 Flexible core-shell/bead-like alginate@PEI with exceptional adsorption capacity, recycling performance toward batch and column sorption of Cr(VI). *Chem. Eng. J.* **313**, 475–486.

Yang, D., Wang, L., Li, Z., Tang, X., He, M., Yang, S., Liu, X. & Xu, J. 2020 Simultaneous adsorption of Cd(II) and As(III) by a novel biochar-supported nanoscale zero-valent iron in aqueous systems. *Sci. Total Environ.* **708**, 134823.

Zhang, R., Ma, H. & Wang, B. 2010 Removal of chromium(VI) from aqueous solutions using polyaniline doped with sulfuric acid. *Ind. Eng. Chem. Res.* **49**, 9998–10004.

Zhang, S. H., Wu, M. F., Tang, T. T., Xing, Q. J., Peng, C. Q., Li, F., Liu, H., Luo, X. B., Zou, J. P., Min, X. B., Luo, J. M., Wu, M. F., Tang, T. T., Xing, Q. J., Peng, C. Q., Li, F., Liu, H., Luo, X. B., Zou, J. P., Min, X. B. & Luo, J. M. 2018 Mechanism investigation of anoxic Cr(VI) removal by nano zero-valent iron based on XPS analysis in time scale. *Chem. Eng. J.* **335**, 945–953.

Zhou, T., Li, C., Jin, H., Lian, Y. & Han, W. 2017 Effective adsorption/reduction of Cr(VI) oxyanion by halloysite@polyaniline hybrid nanotubes. *ACS Appl. Mater. Interfaces* **9**, 6030–6043.

First received 17 March 2023; accepted in revised form 2 October 2023. Available online 12 October 2023